Chapter 12

Fluorescence Lifetime-Based Optical Molecular Imaging

Anand T.N. Kumar

Abstract

Fluorescence lifetime is a powerful contrast mechanism for in vivo molecular imaging. In this chapter, we describe instrumentation and methods to optimally exploit lifetime contrast using a time domain fluorescence tomography system. The key features of the system are the use of point excitation in free-space using ultrashort laser pulses and non-contact detection using a gated, intensified CCD camera. The surface boundaries of the imaging volume are acquired using a photogrammetric camera integrated with the imaging system, and implemented in theoretical models of light propagation in biological tissue. The time domain data are optimally analyzed using a lifetime-based tomography approach, which is based on extracting a tomographic set of lifetimes and decay amplitudes from the long time decay portion of the time domain data. This approach improves the ability to locate in vivo targets with a resolution better than conventional optical methods. The application of time domain lifetime multiplexing and tomography are illustrated using phantoms and tumor bearing mouse model of breast adenocarcinoma. In the latter application, the time domain approach allows an improved detection of fluorescent protein signals from intact nude mice in the presence of background autofluorescence. This feature has potential applications for longitudinal pre-clinical evaluation of drug treatment response as well as to address fundamental questions related to tumor physiology and metastasis.

Key words: Fluorescence, lifetime, fluorescent proteins, optical tomography, tissue optics.

1. Introduction

Optical molecular imaging offers several advantages over conventional techniques such as positron emission tomography (PET) and magnetic resonance imaging (MRI). Foremost among these is cost effectiveness, portability, and the lack of radiation damage. In addition, a wide range of optical probes have been synthesized that allow the ability to multiplex based on fluorescence

K. Shah (ed.), *Molecular Imaging*, Methods in Molecular Biology 680,
DOI 10.1007/978-1-60761-901-7_12, © Springer Science+Business Media, LLC 2011

spectrum and lifetime. In addition to extrinsic targeting of disease using conjugated fluorophores, intrinsic contrast can also be achieved using fluorescent proteins (FPs). FPs are powerful tools for imaging gene expression and tracking disease progression such as metastasis (1, 2). While multi-spectral techniques have been employed to enhance deep tissue fluorescence imaging (3, 4), the application of fluorescence lifetime has been restricted mainly to microscopy techniques (5). For example, a major confound for deep tissue, whole-body imaging of fluorescent proteins is that their excitation wavelength is in the visible region (400–650 nm), and can overlap strongly with tissue autofluorescence (AF) (6). While multi-spectral techniques can be used to alleviate this problem to some extent (4), fluorescence lifetime contrast is an additional mechanism that can improve the separation of the FP signal from background AF using their distinct temporal responses on the nanosecond timescales. More general applications of whole-body lifetime-based molecular imaging are only beginning to emerge in recent years (7, 8). A major challenge for lifetime imaging for deep tissue applications is the technical complexity involved in time domain (TD) instrumentation and in the interpretation of the data. In this chapter, we describe the experimental and theoretical steps involved in obtaining three-dimensional in vivo distributions of multiple lifetimes present within an imaging sample from TD fluorescence measurements.

2. Materials

2.1. Tomography System

A schematic of a free-space, non-contact small animal fluorescence molecular imaging system is shown in **Fig. 12.1**. The main components of the tomography system are an excitation source, detection apparatus, and a 3D camera for surface boundary acquisition. In the non-contact geometry, the sample to be imaged (animal or subject) is placed on a transparent plate directly below the camera and is excited either from below or above using a fiber that delivers the light output of the laser. The individual components are detailed below.

2.2. Excitation and Detection

1. For time domain measurements, a pulsed laser source (<50 ps pulse duration) is necessary. The most versatile excitation sources for NIR measurements are based on Ti:Sapphire lasers for excitation in the near infrared (such as the Mai Tai, Newport-Spectra Physics, Mountain View CA, ~150 fs pulse width, 80 MHz repetition rate, 690–1,020 nm tuning range) or fiber lasers for visible to

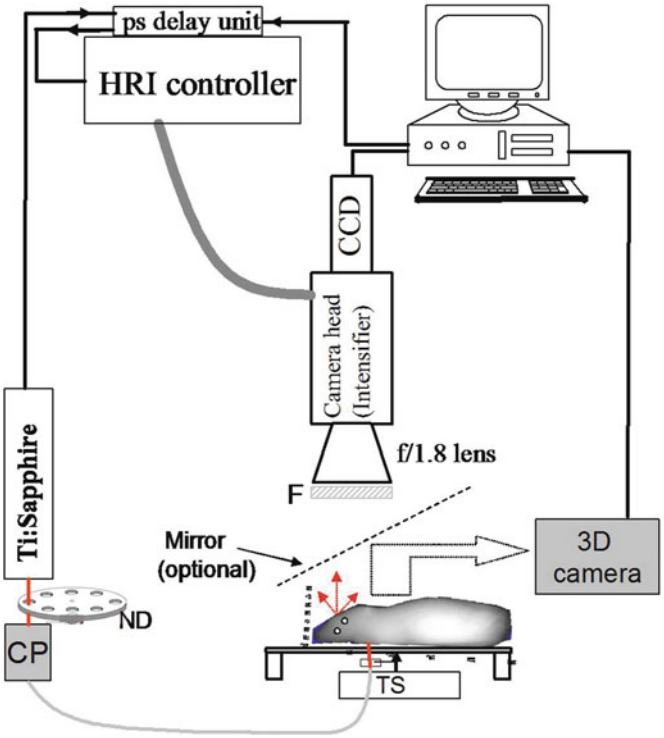

Fig. 12.1. Schematic of the free space TD fluorescence tomography system. The source consists of a Ti:Sapphire laser (750–850 nm), the output of which is collimated using a collimation package (CP) and launched into a 200-μm step-index fiber. The other end of the fiber is connected to a collimation package, to allow for a tight focus spot (1 mm) on the sample surface, and mounted on a translation stage (TS) for scanning over the surface of the imaging subject (*see* **Note 1**). Detection is performed using an intensifier in conjunction with a CCD camera mounted on a manually adjustable rail system. The other symbols are as follows – F: filter (optional); ND: Neutral density filter wheel.

infrared excitation (such as the Fianum, from Fianium Inc., Southampton UK).

2. The light output from the pulsed source is attenuated to about 10 mW depending on the sample thickness, and launched into an SMA connectorized fiber using a fiber collimation package (FC) (Thorlabs Inc.).
3. Using a second collimation package, the light at the output end of the fiber is focused to a fine spot on the imaging surface, resulting in an approximately point excitation source.
4. For tomographic scanning, the second collimation package system is mounted on a computer-controlled, micrometer precision XY translation stage system (Velmex Inc., Bloomfeld NY).

5. The detection is performed in free space using a CCD camera (Picostar HR-12 CAM 2, LaVision GmbH, Goettingen, Germany, quantum efficiency of 65%).
6. A time gated image intensifier (Picostar HR-12, LaVision GmbH, Goettingen, Germany), with a 200 ps minimum gate width, provides nanosecond time resolution.
7. A fast delay unit (Picostar HRI, 1 ms switching, 25 ps minimum steps) is used to delay the trigger output from that of the laser, across one duty cycle of 12.5 ns (80 MHz).
8. The output of the delay unit is in-turn used to trigger the intensifier unit.
9. A camera lens (AF Nikkor, f2.8, Nikon) mounted on the CCD camera is used to obtain a well-focused image of the entire surface of the mouse head on the CCD image plane.
10. A 2 in. interference filter can optionally be mounted to the front of the camera lens to allow excitation or emission measurements (*see* below).
11. Since the scanning speed of the stepper motor is much slower than the delay switching time, the full temporal signal can be collected for one source position at a time (*see* **Note 2**).

2.3. Surface Boundary Acquisition

For accurate forward modeling of the light propagation, the boundary information of the phantom or animal is necessary. Photogrammetric 3D camera systems (such as the 3D Facecam 100, Technest Holdings Inc., Bethesda MD) may be employed to acquire the surface image. The 3D image is acquired by sliding a mirror in front of the camera lens as shown in **Fig. 12.1**. Further details on processing the 3D camera image and co-registration with the CCD image are presented in Section **3** below.

3. Methods

The tomographic reconstruction of fluorescence distribution is achieved using several steps as shown schematically in **Fig. 12.2** (*see* **Note 6**).

1. The TD data comprise of the full temporal profile for multiple sources and detectors (CCD camera pixels) on the surface of the imaging subject. A typical measurement set includes two wavelengths, λ_x and λ_m, which correspond to the absorption and emission maxima of the fluorophore employed for contrast enhancement. Excitation measurements, denoted as $U^{(x,x)}$ and $U^{(m,m)}$, correspond to the

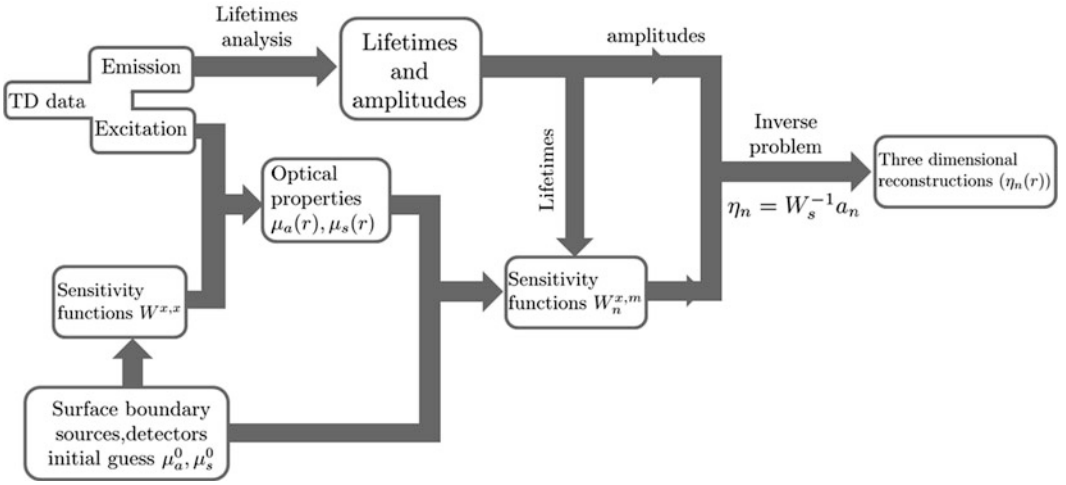

Fig. 12.2. Schematic representation of the steps involved in processing time domain fluorescence data for tomographic reconstructions.

direct detection of light transmitted through the sample at wavelengths λ_x and λ_m and are first acquired with the filter wavelength matching the laser excitation.

2. Emission data (denoted as $U^{(x,m)}$) refer to purely fluorescence emission and are collected with the laser tuned to λ_x, whereas the filter is tuned to λ_m.
3. The excitation and emission data are processed along independent paths. The excitation data are used to determine the background optical property distribution of the sample and to generate sensitivity functions for reconstructing the fluorescence. In parallel, the emission data are analyzed using multi-exponential analysis to recover the amplitudes of all the lifetime components present in the sample.
4. Finally, these amplitudes are used along with the sensitivity functions to invert the 3D yield distribution for each lifetime component. The individual steps are further detailed below.

3.1. Measuring the Impulse Response, Time Origin, and Source Positions

1. The system impulse response function (IRF) is defined as the signal at the detector in the absence of any sample. The IRF can be readily measured by placing a thin, non-scattering absorber, such as a piece of paper on the imaging plate (without the sample). The signal collected at the camera then directly gives the IRF. The IRF provides information for the initial time t_0 when the excitation pulse is incident on surface of the imaging medium. A correct estimate of t_0 ensures that the relative amplitudes of the multiple lifetime components are correct, and is crucial for estimating the optical properties using TD data.

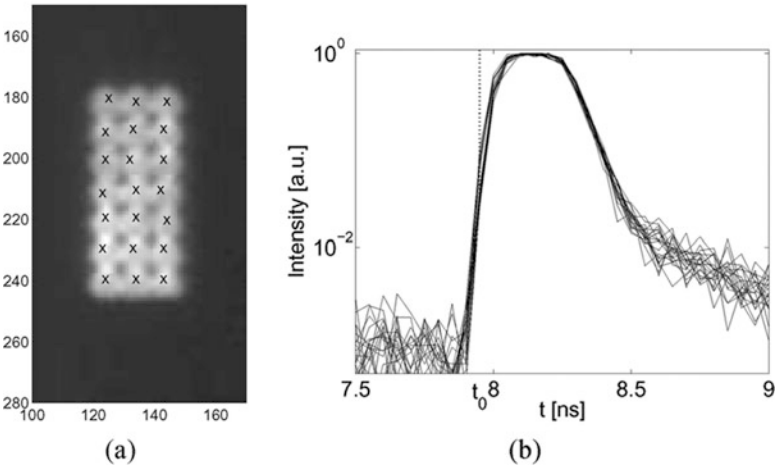

Fig. 12.3. Measurement of IRF and time origin. **a** Direct CCD image of the source illumination, obtained by focusing the fiber output on a thin sheet of paper placed on the imaging plate (without the imaging subject present). The image shown is the integrated TD signal for 21 source positions, used for the phantom measurements reported in the text. The source coordinates were obtained as the points of maximum intensity. **b** Normalized TD Impulse response curves for all the 21 sources. The *vertical dotted line* indicates the time origin t_0, estimated as the time at 1% of the peak intensity. The time t_0 corresponds to the initial time of excitation at the boundary of a subject placed on the plate, assuming the subject surface is approximately flat. Reproduced from Kumar et al., with permission from IEEE (© 2008, IEEE) (13).

2. **Figure 12.3a** shows the time integrated, i.e., continuous wave (CW) IRFs for a grid of 21 source positions spaced 2 mm along the X and Y translation directions. The source grid image in **Fig. 12.3a** also serves to determine the coordinates of the sources for forward modeling. These are obtained as the points of maximum intensity, after the image for each source position is median-filtered.
3. **Figure 12.3b** shows the corresponding IRF's for all source positions. The width of the IRF is ideally nearly equal to the gate width setting of the intensifier unit. Since the variation between the IRF is minimal across the sources (<10 ps), the initial time t_0 can be assumed to be identical for all source positions and estimated from the mean of the impulse response as the time at 1% of the peak. This value can be assumed to be the excitation time at the surface of the imaging medium provided the boundary of the imaging volume is approximately flat (*see* **Note 3**).
4. The measured IRF can be directly forward convolved into the model before tomographic inversion. (This procedure is superior to a de-convolution of the IRF from the raw fluorescence data, which is a highly ill-posed problem.)

3.2. Surface Boundary and Co-registration

1. The imaging subject is placed on the imaging plate and its boundary secured using additional restraints for repeatability in positioning.
2. The 3D image surface is then acquired with the optional mirror in place (**Fig. 12.1**).
3. The 3D camera captures a surface image of the mouse as triangulated vertex data with a resolution of 100 μm. This high-density data are first reduced to a set of unique surface mesh points, which are then interpolated using the Matlab (The Mathworks, Natick, MA) function "ndgrid," to provide a surface on a uniform mesh.
4. The surface image is then co-registered with the planar image of the CCD camera with which the fluorescence data are acquired. The transformation can be effected as a 2D affine transformation between the CCD image and the 3D surface image, using four fiducial points in the form of metal screws placed on the subject plate at points identifiable both in the 3D camera and the CCD field-of-view (indicated by a "+" sign in **Fig. 12.4**).
5. Once the affine transformation matrix between the 3D camera image and the CCD image has been determined, the source and detector locations are transformed to the reference frame of the 3D camera image. The surface data are next converted into an indexed volume image and used in numerical modeling of light transport (*see* **Note 4**).
6. A single 3D image thus acquired along with the fiducials can be used as the reference image for any optical measurement using the same subject provided that the fiducial points are visible on the CCD image and the subject is placed at the same relative position with respect to the fiducials.

Figure 12.4 shows the co-registration results for a mouse shaped phantom. **Figure 12.4a** shows the CCD image with the mouse phantom, the fiducials, and a grid of 93 detector positions arranged on the camera image. **Figure 12.4b** shows the planar image of the 3D surface used for the co-registration, along with source and detector coordinates mapped on the surface image using the affine transformation.

3.3. Multi-exponential Fits

We envisage a scenario where a single or multiple fluorophore(s) are injected into an animal and the in vivo distribution of each lifetime component of the fluorophore(s) can reveal potential information about the disease target. To proceed with the analysis, a key step is the extraction of the lifetimes and the decay amplitudes as measured on the surface. As shown in **Fig. 12.2**, this proceeds independently of the optical property estimation.

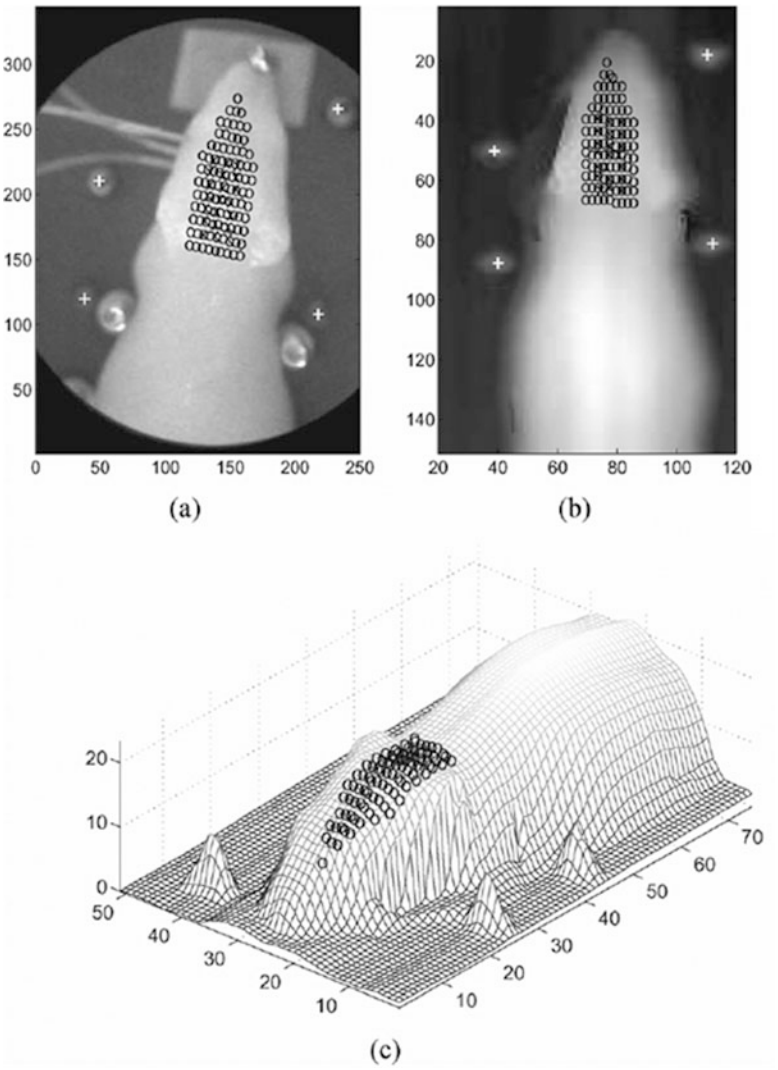

Fig. 12.4. Coregistration of CCD camera image with 3D camera surface image. **a** Room light illuminated image of the mouse phantom placed on the imaging plate. The + symbols indicate the fiducial points used for co-registration. The sources (x) determined from the impulse response (*see* **Fig. 12.3**) and detectors (o) assigned on the camera image also shown. **b** *Top-down* view of the 3D surface of the mouse phantom, also showing the fiducials (+) and the mapped sources and detectors, whose coordinates were determined from the affine transformation (**Section 3.2**). **c** 3D view of the surface image of the phantom shown along with the transformed detectors from the CCD image. Reproduced from Kumar et al., with permission from IEEE (© 2008, IEEE) (13).

1. According to the asymptotic model (9), the measured fluorescence signal, $U(x,m)$, can be expressed in the asymptotic limit as a sum of discretized exponential decays with lifetime components, τ_n, which are independent of the measurements locations (i.e., the S-D coordinates):

$$U^{(x,m)}(\mathbf{r}_s, \mathbf{r}_d, t) \rightarrow \sum\nolimits_n a_n(\mathbf{r}_s, \mathbf{r}_d) e^{-t/\tau_n} \quad [1]$$

where $\mathbf{r}_s$ and $\mathbf{r}_d$ are the coordinates of the source and detector. The amplitudes, a_n, which can be recovered simply by fitting the decay portion of the time domain data, are directly related to the spatial distribution of the fluorophore corresponding to that lifetime, labeled as $\eta_n(r)$. The nonlinear fits to recover the lifetimes and amplitudes are numerically implemented using built-in Matlab functions such as "fminsearch," which employs an unconstrained nonlinear optimization using the Nelder-Mead simplex approach (*see* **Note 5**).

2. In some applications (such as autofluorescence and other complex fluorophores), the fluorescent target of interest may exhibit non-exponential behavior, i.e., cannot be described by a single exponential decay function. In this case it is more appropriate to analyze the fluorophore in terms of basis functions that have been pre-determined. One example is tissue autofluorescence (*see* equation [4] and related discussion in **Section 3.9**).

3.4. Optical Property Estimation and Sensitivity Functions

With a knowledge of source-detector locations in the reference frame of the 3D digitized volume of the imaging subject, the next step is the computation of the "forward problem," which involves modeling the light propagation within the tissue volume. This can be carried out either using a transport equation-based approach, numerically implemented using the Monte-Carlo (MC) method (10, 11) or a diffusion-equation based approach implemented using the finite element method (FEM) (12).

1. The forward problem is calculated with an initial assumption for the optical absorption, μ^0 and scattering, μ^0 coefficients, usually assumed to be homogeneous throughout the sample volume.
2. The computational prediction from the model is then matched with the measured excitation measurements ($U^{(x,x)}$ and $U^{(m,m)}$) using iterative fitting procedures to obtain heterogeneous distributions of the absorption and scattering $\mu_a(r)$ and $\mu_s(r)$, at λ_x and λ_m, where r denotes the position within the imaging sample.
3. The continuous-wave fluorescence sensitivity functions for each lifetime component, $W^{(x,m)}$, are then calculated using the heterogeneous absorption reduced by $1/v\tau_n$, i.e., $\mu_a(r) - 1/v\tau_n$, where v denotes the velocity of light in the medium (13). These sensitivity functions will be later used to recover the fluorescence distribution for each lifetime component as detailed below.

3.5. Inverse Problem and Tomographic Reconstruction

The amplitudes recovered from the asymptotic approach (**Section 3.3**) are directly related to the fluorescence sensitivity profiles $W^{(x,m)}$ (**Section 3.4**) and the fluorescence distributions for each lifetime $\eta_n(r)$ as follows:

$$a_n(\mathbf{r}_s, \mathbf{r}_d) = \int d^3 r W_n^{(x,m)}(\mathbf{r}_s, \mathbf{r}_d, \mathbf{r}) \eta_n(\mathbf{r}). \quad [2]$$

The above equation needs to be solved for the unknown fluorescence yield distributions $\eta_n(\mathrm{r})$. Denoting $W_n^{(x,m)}$ as W for simplicity, the inverse solution is written as $\eta_n = W_s^{-1} a_n$, where the pseudo-inverse of the sensitivity function defined as

$$W_s^{-1} = W^T (WW^T + \alpha\lambda I)^{-1} \quad [3]$$

where $\alpha = \max(\mathrm{diag}(WW^T))$. Various conditioning techniques may be employed to improve the quality of the reconstruction (12).

3.6. Mouse Phantoms

1. Mouse shaped phantoms are prepared using the negative mold made from a sacrificed mouse. The mold for the phantom consists of a two-part epoxy resin (7132) and hardener (2001) mixture, from Douglas & Sturgess Inc. (San Francisco, CA).
2. First, calculate the net volume of the mold to be filled. Then weigh two parts of the resin and one-part hardener by weight in separate containers, and mix them thoroughly.
3. Next, add a combination of TiO_2 (paint) and ink to the epoxy-resin mixture, to achieve approximate background optical properties of $\mu_s = 10\ \mathrm{cm}^{-1}$ and $\mu_a = 0.1\ \mathrm{cm}^{-1}$. Mix thoroughly.
4. Inclusions (cavities) can be created inside the phantom by positioning low-melting-point agar beads (5 mm diameter) using pairs of syringe needles. The agar beads can be cast in a spherical negative mold.
5. Pour the epoxy mixture into the negative mold and let it cure for about 12 h.
6. Once the mold is cured, remove the needles and the negative mold. Next, attach fresh needles along with polypropylene tubing, to enable dynamic injection of fluorophores into the inclusions. **Figure 12.5a** shows a photograph of the mouse phantom along with the injection tubes.

3.7. Cell Culture Preparation and Tumor Mice Models

1. Tumor bearing mouse models were derived from the human breast cancer cell line, MDA-MB-231, which expressed both enhanced green fluorescent protein (EGFP) and cyan fluorescent protein (CFP).

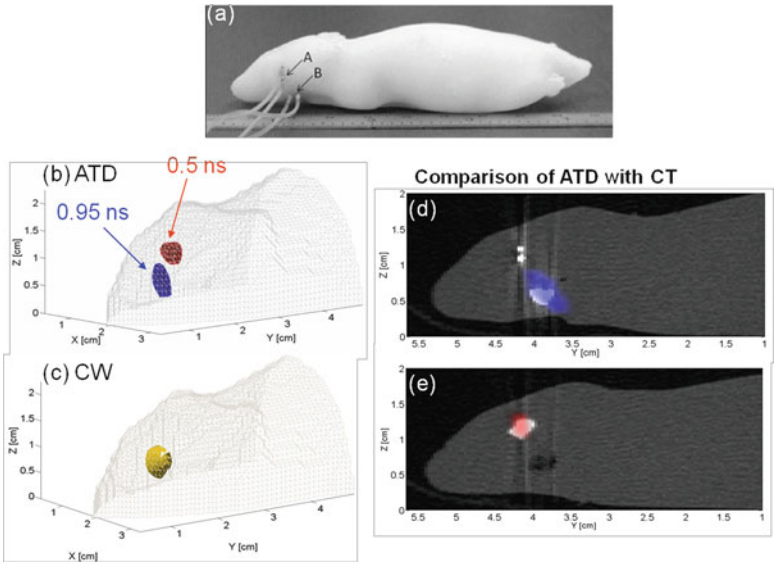

Fig. 12.5. Phantom validation of lifetime based tomography. **a** The phantom (epoxy+Ti02+ink combination) had two inclusions (*A* and *B*) for fluorophore injection. **b** TD reconstruction of data collected with the two inclusions filled with a NIR dye in water (0.5 ns) and glycerol (0.95 ns). The reconstructed yields are shown for 0.5 ns (*red*) and 0.95 ns (*blue*) as iso-surfaces at 95% the maximum intensity. The gray mesh is the 3D surface (from the 3D camera) used for the forward modeling. **c** The CW reconstruction does not resolve the two inclusions separately. The ATD reconstruction are shown **d** for the 0.95 ns component (*blue*) and **e** for the 0.5 ns component (*red*), co-registered with the CT images of the phantom (*grayscale*, with inclusions seen as *white*). The images in (d) and (**e**) show sagittal planes containing the centroid of the two inclusions. (The two tubes feeding inclusion *A* are visible in (d).)

2. Cells are first grown in a humidified atmosphere under 5% CO_2. The cells ($\approx 2 \times 10^6$) are then suspended in 50 µl of Hanks' Balanced Salt Solution (Invitrogen, New York).
3. For in vitro studies, the cells are placed in eppendorf tubes and imaged in a reflectance model with the TD system.
4. For in vivo imaging, the tumor cells are injected directly into the mammary fat pads of 6- to 8-week-old female nude mice.
5. The mice are imaged 3–4 weeks post implantation, when the tumor is 7−8 mm in diameter.

3.8. Tomography with Mouse Phantoms

1. **Figure 12.5** shows a demonstration of lifetime-based tomography in a mouse shaped phantom. The phantom had two approximately spherical inclusions (**Fig. 12.5a**), filled with a NIR dye (3,3′-diethylthiatricarbo-cyanine) with absorption and emission maxima near 755 and 790 nm.
2. To achieve lifetime contrast, two solutions were prepared with the dye dissolved in distilled water and glycerol solutions, which resulted in intrinsic lifetimes of 0.5 and 0.95 ns, respectively (13).

3. The longer lived dye solution in glycerol was injected in inclusion B and the shorter lived aqueous dye solution of the dye in inclusion A (*see* **Fig. 12.5a**). The mouse phantom was placed in the imaging setup shown in **Fig. 12.1** and the data were collected in the trans-illumination geometry for 21 source positions and 93 assigned detectors on the camera image (source-detector arrangement shown in **Fig. 12.4**).
4. The decay amplitudes for the two lifetime components were inverted to recover the fluorescence yield localizations as prescribed in equations [2] and [3].
5. The reconstruction results using the lifetime-based approach are shown in **Fig. 12.5b** as 3D images overlayed with the surface boundary of the phantom. The images shown are isosurface maps at 95% peak intensity.
6. The regularization parameter λ (equation [3]) was near unity for the reconstructions shown and was chosen based on an empirical assessment of image quality.
7. The yield reconstruction for the shorter lifetime of 0.5 ns is seen to have a shallower depth than that for the longer lifetime of 0.95 ns, as expected.
8. Also shown in **Fig. 12.5c** is the reconstruction of the two inclusions using the CW component of the data, which is unable to resolve the two axially located inclusions. (Further details regarding the accuracy of the reconstructions can be found in reference (12).)
9. The TD reconstructions were compared with CT images of the mouse phantom, to verify accuracy. As seen from **Fig. 12.5d, e**, the asymptotic yield reconstructions match the true locations of the inclusions as recovered by the CT image reasonably well.

3.9. Imaging of Fluorescent Protein Expression in Tumor Bearing Mice

1. **Figure 12.6** shows an example application of lifetime multiplexing for imaging fluorescent protein expressing tumors in a mouse model of breast adenocarcinoma. **Figure 12.6b** shows the CW (intensity only) reflectance image for area illumination across the torso of the mouse placed in supine position, for 488 nm (10 nm width) excitation and 515 nm (long pass) emission. The CW image is overlaid on the white light image of the mouse. While the location of the tumor is apparent from the intensity image, the AF component is significant across the whole illumination area and effectively reduces the contrast of the FP signal.
2. The AF decay is highly non-exponential and has lifetime components overlapping with the FP lifetime, making the two indistinguishable in a multi-exponential analysis approach. Thus, rather than fit the surface TD

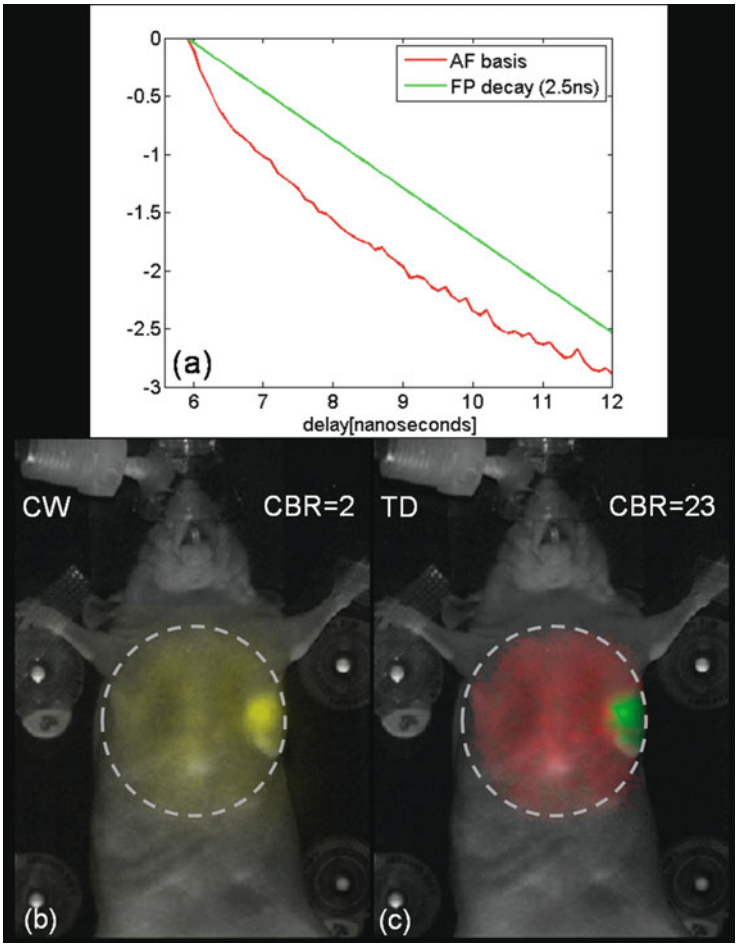

Fig. 12.6. Whole-body fluorescence lifetime measurements with FP expressing tumor mouse models. **a** Temporal responses of the autofluorescence and the dual EGFP/CFP expressing tumor cell lines. The AF decay is non-exponential, described by a basis function $B(t)$ while the FP decay is exponential with a lifetime of 2.5 ns. **b** CW component (*yellow*) of the reflectance TD fluorescence measurement (exc:488 nm, em:515 nm longpass) of an anesthetized nude mouse placed in supine position. 2×10^6 EGFP/CFP expressing breast tumor cell lines (MDA-MB-231) were implanted in the mammary fat pad. The images shown were obtained 3 weeks post implantation. **c** The amplitude components of the AF (*red*) and FP (*green*) decays, *a*AF and *a*FP, obtained by fitting equation [4] to the raw TD fluorescence data are shown as a single RGB image. The *dashed lines* indicate the illumination area ($\approx$2.5 cm^2). The background image of the mouse is shown in *grayscale*.

decays to a sum of exponentials, more robust results can be obtained using a "basis function" approach that performs a linear fit for the decay amplitudes, using a priori knowledge of the decay profiles of the AF and FP.

3. First, the FP lifetimes can be easily measured in vitro using the tumor cells prior to injection into the mice. The lifetime

of the dual EGFP/CFP expressing cells used here was found to be 2.5 ns.

4. Second, the AF basis function was formed as the average AF response (for 488 nm excitation/515 nm long pass detection, corresponding to the FP excitation and emission) across the torso of three mice. **Figure 12.6a** shows the decay profiles of the AF and the FP fluorescence used as basis functions. Using the known FP lifetime and the AF basis $B(t)$, a simple bi-functional linear model was used to fit the asymptotic portion (8) of the raw TD data:

$$U(\mathbf{r}_d, t) = a_{\mathrm{AF}}(\mathbf{r}_d)B(t) + a_{\mathrm{FP}}(\mathbf{r}_d)\exp(-t/\tau_{\mathrm{FP}}), \quad [4]$$

where τ_{FP} is the lifetime of the FP and r_d is the location of an image pixel. **Figure 12.6c** shows the decoupled AF (red) and FP (green) amplitudes as the red and green components of a single RGB image matrix. The error of the fit was less than 5% across the entire illumination area. The TD approach (**Fig. 12.6c**) confirms the presence of the tumor and provides a superior delineation of the tumor from the background AF, as compared to the CW intensity image (**Fig. 12.6a**).

5. The contrast-to-background ratio (CBR) was estimated for the CW (TD) approaches as the ratio of the net intensity (decay amplitude) within the tumor region and corresponding value outside the tumor region. The CBR was near 23 for the TD approach, compared to near 2 for the CW case, suggesting a > tenfold improvement.

6. While this example shows that planar lifetime imaging can by itself enable longitudinal quantification of tumor growth, angiogenesis and therapeutic response in a single animal, the FP amplitudes, a_{FP}, could also be employed in lifetime-based tomography techniques as detailed in earlier in **Section 3** for recovering 3D distributions of FP expression.

4. Notes

1. Reflectance measurements could also be readily performed, if needed, by mounting the fiber above the phantom plate (not shown in **Fig. 12.1**).

2. An alternative approach to stepper motor based scanning is the use of gavanometers with millisecond switching times. This will allow whole body scans for each time step.

3. The measured time at the detector pixels is offset from the actual t_0 by the time for free space propagation of light from the source to the camera. When an imaging medium of small thickness, such as a mouse, is placed on the source plate, the corresponding offset for fluorescence emitted on the surface will very nearly equal the offset from the source. A small correction factor can be applied to account for the propagation time in free space corresponding to the thickness of the mouse (e.g., for a 2-cm-thick mouse, the time offset is ≈ 50 ps).
4. If the heterogeneous tissue structure of the animal is available from either MRI or CT scans, these can be employed directly in the approach presented here with appropriate fiducials and co-registration.
5. The recovery of lifetimes from decay data is a non-linear problem that can be computationally challenging, especially for more than two lifetimes. The best-case scenario is when the in vivo lifetimes are known in advance. Alternatively, the multi-exponential analysis can be performed in two stages for robust fitting results. First, an integrated decay function is formed by summing the decays from all S-D pair measurements, to obtain a high signal-to-noise ratio (SNR) temporal data set. This "global" signal is composed of all the lifetime components present in the system, and allows a more robust determination of the lifetimes through a non-linear analysis. In the second step, the lifetimes determined from the surface-integrated time domain data are used in a *linear* fit of the DFTR for each individual S-D pair. Besides improving the robustness of the fitting procedure for the lifetimes and decay amplitudes, the global analysis is computationally much less cumbersome than performing a non-linear fit for every S-D measurement.
6. Other approaches for analyzing time domain fluorescence data have also been presented particularly based on using the early arriving photons for improved resolution (14). This chapter is concerned with fluorescence lifetime contrast which involves the late arriving photons, and provides complementary information regarding the in vivo fluorescence distribution.

Acknowledgement

This research was supported by the National Institutes of Health grant NIH AG026240.

References

1. Jain, R. K., Munn, L. L., and Fukumura, D. (2002) Dissecting tumor pathophysiology using intravital microscopy. *Nat. Rev. Cancer* **2**, 266.
2. Yang, M., et al. (2003) Dual-color fluorescence imaging distinguishes tumor cells from induced host angiogenic vessels and stromal cells. *Proc. Nat. Acad. Sci. USA* **100**, 14259.
3. Gao, X., Cui, Y., Levenson, R. M., Chung, L. W. K., and Nie, S. (2004) In vivo cancer targeting and imaging with semiconductor quantum dots. *Nat. Biotech.* **22**, 969.
4. Tam, J. M., Upadhyay, R., Pittet, M. J., Weissleder, R., and Mahmood, U. (2007) Improved in vivo whole-animal detection limits of green fluorescent protein-expressing tumor lines by spectral fluorescence imaging. *Mol. Imaging* **6**, 269–76.
5. Bastiaens, P. I. H. and Squire, A. (1999) Fluorescence lifetime imaging microscopy: spatial resolution of biochemical processes in the cell. *Trends Cell. Biol.* **9**, 48.
6. Deliolanis, N. C., Kasmieh, R., Wurdinger, T., Tannous, B. A., Shah, K., and Ntziachristos, V. (2008) Performance of the red-shifted fluorescent proteins in deep-tissue molecular imaging applications. *J. Biomed. Opt.* **13**, 044008.
7. Bloch, S., Lesage, F., Mackintosh, L., Gandjbakche, A., Liang, K., and Achilefu, S. (2005) Whole-body fluorescence lifetime imaging of a tumor-targeted near-infrared molecular probe in mice. *J. Biomed. Opt.* **10**, 054003.
8. Kumar, A. T. N., Chung, E., Raymond, S. B., Van de Water, J., Shah, K., Fukumura, D., Jain, R. K., Bacskai, B. J., and Boas, D. A. (2009) Feasibility of in vivo imaging of fluorescent proteins using lifetime contrast. *Opt. Lett.* **34**, 2067.
9. Kumar, A. T. N., Raymond, S. B., Boverman, G., Boas, D. A., and Bacskai, B. J. (2006) Time resolved fluorescence tomography based on lifetime contrast. *Opt. Exp.* **14**, 12255–70.
10. Wang, L., Jacques, S. L., and Zheng, L. (1995) MCML-Monte Carlo modeling of light transport in multi-layered tissues. *Comput. Methods Programs Biomed.* **47**, 131–46.
11. Boas, D. A., Culver, J. P., Stott, J. J., and Dunn, A. K. (2002) Three dimensional Monte Carlo code for photon migration through complex heterogeneous media including the adult human head. *Opt. Exp.* **10**, 159–70.
12. Arridge, S. R. (1999) Optical tomography in medical imaging. *Inverse Probl.* **15**, R41–93.
13. Kumar, A. T. N., Raymond, S. B., Dunn, A. K., Bacskai, B. J., and Boas, D. A. (2008) A time domain fluorescence tomography system for small animal imaging. *IEEE Trans. Med. Imaging* **27**, 1152.
14. Niedre, M. J., de Kleine, R. H., Aikawa, E., Kirsch, D. G., Weissleder, R., and Ntziachristos, V. (2008) Early photon tomography allows fluorescence detection of lung carcinomas and disease progression in mice in vivo. *Proc. Natl. Acad. Sci. USA* **105**, 19126–31.